www.sciencemag.org/cgi/content/full/341/6149/1016/DC1

Supplementary Materials for

βCaMKII in Lateral Habenula Mediates Core Symptoms of Depression

Kun Li, Tao Zhou, Lujian Liao, Zhongfei Yang, Catherine Wong, Fritz Henn, Roberto Malinow, John R. Yates III, Hailan Hu*

*Corresponding author. E-mail: hailan@ion.ac.cn

Published 30 August 2013, *Science* **341**, 1016(2013)
DOI: 10.1126/science.1240729

This PDF file includes

Materials and Methods

Animals. Male cLH rats (4 - 7 weeks of age) and age-matched male Sprague Dawley rats (purchased from Shanghai SLAC Laboratory Animal Co.) were used. The cLH rats were bred as previously described (*40*). The rats were housed two/cage under a 12-h light-dark cycle (light on from 7 a.m. to 7 p.m.). Male adult (10-14 weeks of age) C57BL/6 mice (SLAC) were used for behavioral tests. Mice were group-housed four/cage under a 12-h light-dark cycle (light on from 5 a.m. to 5 p.m.). Both rats and mice were housed in stable conditions with food and water *ad libitum*. All animal studies and experimental procedures were approved by the Animal Care and Use Committee of the Institute of Neuroscience, Chinese Academy of Sciences.

Proteomics. Three pairs of brain samples from naive wild type SD rats and congenital learned helpless (cLH) rats which displayed depressive-like behaviors in both learned helpless and forced swimming tests were used for proteomic analysis. Rats were anesthetized by isoflurane and brains were removed. Habenular tissue was quickly hand dissected and frozen with liquid nitrogen. Habenular tissue from different samples and whole brain from ^{15}N rats (rats that have been on ^{15}N diet for two generations so that the atomic enrichment of ^{15}N reached $\geq$ 94%(*41*)) were homogenized in ice-cold homogenization buffer (320 mM sucrose, 4 mM HEPES pH 7.4, 1 mM $MgCl_2$ and 0.5 mM $CaCl_2$, 5 mM NaF, 1 mM Na_3VO_4, EDTA-free, Protease Inhibitor cocktail tablets (Roche) using glass homogenizers. After protein concentration measurement by Bradford assay, the sample homogenates were mixed with ^{15}N-labeled rat brain homogenate in a 1:1 (w/w) protein ratio respectively. The mixture was centrifuged at 800g for 15 min at 4°C. The supernatant was taken and then centrifuged at 10,000g for 15 min. The pellet was the crude membrane fraction and dissolved in homogenization buffer. One hundred micrograms of protein samples were digested and then analyzed by Multidimensional Protein Identification Technology (MudPIT)(*42*). For each identified protein, the intensity ratio between ^{14}N peptides and ^{15}N peptides was calculated at the peptide level and averaged at the protein level. The ratios of thousands of proteins for each sample run were log (Ln) transformed to obtain a normal distribution, and normalized by shifting the median log ratio to 0. After normalization, the protein ratio of cLH verse that of control was the protein fold change in depression. Significance value was calculated as the average normalized ratio minus two folds of standard deviation for each protein (fig. S1A). Proteins with change of more than $\geq$ 50% and significance value > 0 were selected for further validation. Student's *t* test was performed on the log transformed fold change ratios for each protein to derive the p value in table S1.

Constructs and viral packaging. For AAV viruses, the AAV-βCaMKII-2A-EGFP, AAV-αCaMKII-2A-tdTomato, AAV-βCaMKII-K43R-2A-EGFP, AAV-βCaMKII-2A-Glu-R1Ct, AAV-GFP-CRE and AAV-GFP plasmids were all designed and constructed by standard methods. Full length cDNAs of βCaMKII and αCaMKII were transcribed from SD rat cDNA library. The sequence of 2A signal peptide was derived from plenti-2A-EGFP plasmid. AAV2 backbone was cloned from AAV-GFP-CRE plasmid (gift from Lisa Monteggia). For AAV-βCaMKII-2A-EGFP plasmid, βCaMKII was first inserted into plenti-Ubiquitin-2A-EGFP plasmid, then Ubiquitin-βCaMKII-2A-EGFP was inserted into AAV backbone with BglII and XhoI. αCaMKII was cloned into pLenti-2A-tdTomato vector with BamH1 and Xba1. αCaMKII-2A-tdTomato was

amplified by PCR from Lenti vector and then ligated with AAV vector using Xbal1 and BsrG1 enzymes. For AAV-βCaMKII-K43R-2A-EGFP, βCaMKII-K43R (gift from Yizheng Wang) was subcloned into AAV-2A-EGFP with XbaL1 and EcoR1. For AAV-βCaMKII-2A-EGFP-GluR1Ct plasmid, the EGFP-GluR1Ct fragment was amplified from pSindbis-EGFP-GluR1Ct plasmid, then ligated with AAV-βCaMKII-2A fragment. The AAV-βCaMKII–RNAi was constructed using a vector (provided by Neuron Biotech company, Shanghai), which contains a CMV promoter driving EGFP and a H1 promoter driving shRNA expression. The sequence of βCaMKII shRNA is 5'-GAGTATGCAGCTAAGATCA-3'. The AAV2 helper vectors, pXX680 and pXX2 were purchased from University of North Carolina at Chapel Hill. The AAV2 viruses were generated as previously described (*43*). In brief, HEK293TN cells were transfected with two helper vectors, pXX680 and pXX2 and one AAV vector. 48 hours after transfection, virus was purified from the cell lysate by using a heparin-agarose column and concentrated to the final volume. The virus titer was measured by infecting HEK293TN cells with 10 times gradient diluted virus.

Antidepressant treatment. Antidepressant treatment of cLH rats was achieved by i.p. injection of Imipramine (10 mg/kg, Sigma) for 14 days. The day after the last injection, learned helplessness test was conducted. Two days after the behavioral test, brain samples were taken for Western analysis.

Stereotactic injection and Histology. For viral injection, mice were anesthetized with ketamine (100 mg/kg of body weight) and xylazine (8 mg/kg) by i.p. injection and placed in a stereotactic frame. Mice were injected bilaterally with 0.8 ~ 1 μl of purified and concentrated AAV virus (~10^{12} infections units per ml) into the LHb (coordinates from bregma: −1.32 mm anterior/posterior, ±1.04 mm medial/lateral, −2.48 mm dorsal/ventral, with 14° angle toward the midline in the coronal plane) using glass microelectrodes at a slow rate (~100-150 nl/min). The injection microelectrode was slowly withdrawn 5min after the virus infusion. For viral injections in rats, rats were anesthetized with 10% chloral hydrate (4ml/kg of body weight, i.p. injection) and injected bilaterally with 1~1.5μl of AAV virus into the LHb (for SD rats at age 4 weeks, AP, -3.0 mm from bregma; ML, ±0.7 mm; DV, -4.4 mm from bregma; for cLH rats at age 4 weeks, AP, -3.0 mm from bregma; ML, ±0.7 mm; DV, -4.55 mm from bregma; for cLH rats at age 6 weeks, AP, range from -3.3 mm from bregma; ML, ±0.7 mm; DV, -4.7 mm from bregma). Little labeling was observed in the microelectrode tract. Behavior experiments or electrophysiological recordings were performed at least 7 days after surgery. The injection sites were examined at the end of all the behavior tests and only data from animals with correct injections were included. Brain slices from mice or rats injected with AAV-αCaMKII-tdTomato were directly examined under fluorescent microscope. Brain slices from mice or rats injected with all other GFP labeled viruses were stained with antibody against GFP before microscopic examination. Each brain was sectioned into 6 serials slices for habenula region (mice 30 μm slice, 6 slices per serial; rats 40 μm slice, 8 - 9 slices per serial). All slices were counterstained with Hoechst before mounting on the slides. The infection rate was calculated for LHb region. For each animal, infection rate counting was conducted in one serial slices from anterior to posterior using ImageJ. Numbers of total neurons in one region were averaged from counting NeuN signals in parallel serial slices of two control animals. Infection rate was derived by dividing the number of infected cells by that of total neurons.

Immunohistochemistry and Western blot. For perfusion, mice or rats were deeply anesthetized by using 10% chloral hydrate and perfused with phosphate-buffered saline (PBS) followed by 4% paraformaldehyde in PBS. Brains were post-fixed overnight in the same 4% paraformaldehyde solution and cryoprotected by immersion in 30% sucrose solution (in PBS) for 1 day (for mice) or 3 days (for rats). Frozen brains were sectioned at 30 μm (mice) or 40 μm (rats) with a sliding microtome (CM1950, Leica) in the coronal plane. Slices were immersed in PBS and stored at 4 °C for further using. The antibodies used were rabbit anti-CaMKII (1:300, Epitomics), rabbit anti-GluR1 (1:300, Chemicon), mouse anti-NeuN (1:1000, Chemicon), rabbit anti-GFP (1:1000, Invitrogen), chicken anti-GFP a (1:1000, ABCAM), Alexa Fluor488 goat anti-rabbit IgG, Alexa Fluor488 goat anti-chicken IgG, Alexa Fluor594 goat anti-mouse IgG (all 1:1000, Invitrogen), Biotinylated Goat anti-rabbit IgG, Biotinylated Goat anti-mouse IgG (all 1:250, Vector laboratories), Cy3-conjugated Streptavidin, Cy2-conjugated Streptavidin (all 1:1000, Jackson ImmunoResearch). Especially for CaMKII and GluR1 staining, we used the three-step amplification protocol. Slices were sequentially incubated with anti-CaMKII or anti-GluR1 antibody and Biotinylated Goat anti-rabbit or anti-mouse IgG, finally the Cy3 or Cy2-conjugated Streptavidin. All slices were counterstained with Hoechst in the final step incubation. Fluorescent image acquisition was performed with an Olympus Fluoview FV1000 confocal microscope using 10X and 20X objective lens and on an Olympus MVX10 microscope using MV PLAPO 2XC objective. Images were analyzed using Image-Pro Plus and ImageJ software. For CaMKII and GluR1 fluorescence intensity quantification, 20X confocal images of virus injected side and un-injected side of LHb were acquired using identical settings and further analyzed using Image-Pro Plus. The Integrated Optical Density (IOD) of IHC signals was divided by area value of Hoechst signals to derive the fluorescence signal intensity. Fluorescence intensities of the viral injected and un-injected side of LHb were compared to get the over-expression level.

For Western blot, processing of habenula or hippocampal tissue is the same as that used in mass spectrometry. 8~15 μg proteins were loaded on each lane and electrophoretically separated on an SDS-PAGE gel (10%) and transferred for Western blot analysis. The antibodies used were anti-βCaMKII (1:1000, Invitrogen), anti-αCaMKII (1:2000, Millipore), anti-γCaMKII (1:1000, PTG), anti-δCaMKII antibody (1:500, Santa Cruz), anti-GluR1(1:1000, Millipore) and anti-tubulin antibody (1:10000, Bio-Rad). High sensitive ECL reagent was used (GE Healthcare).

Slice preparation. Sprague Dawley rats (postnatal 40-50 days) were anesthetized with isoflurane and then perfused with 20 ml ice-old dissection buffer (25.0 mM $NaHCO_3$, 1.25 mM NaH_2PO_4, 2.5 mM KCl, 0.5 mM $CaCl_2$, 7.0 mM $MgCl_2$, 25.0 mM glucose, 110.0 mM choline chloride, 11.6 mM ascorbic acid and 3.1 mM pyruvic acid, gassed with 95% O_2 and 5% CO_2). Brain was quickly dissected out after decapitation. Coronal habenular slices (350 μm thick) were sectioned on a vibratome in oxygenated chilled dissection buffer. Then habenular slices were incubated in oxygenated ACSF (118 mM NaCl, 2.5 mM KCl, 26 mM $NaHCO_3$, 1 mM NaH_2PO_4, 10 mM glucose, 1.3 mM $MgCl_2$ and 2.5 mM $CaCl_2$, gassed with 95% O_2 and 5% CO_2) at 32°C to recover for 2 hours and then transferred to the recording chamber with continuous oxygenated ACSF perfusion.

Electrophysiology. Patch-clamp experiments were made from the lateral habenular neurons at 27±1 °C using Multiclamp 700B amplifier under an Olympus microscope equipped with infrared differential interference contrast optics. The pipette resistance was in the range of 3-4 MΩ. For mEPSC recordings, neurons were clamped at -60 mV in the presence of TTX (1 μM) and picrotoxin (100 μM) in ACSF. The intracellular solution contained $CsMeSO_3$ 115mM, CsCl 20mM, HEPES 10 mM, $MgCl_2$ 2.5 mM, Na_2-ATP 4mM, Na-GTP 0.4mM, Na-phosphocreatine 10 mM, and EGTA 0.6 mM. Data was filtered at 2 kHz and sampled at 10 kHz using Digidata 1322A. Pairs of neighboring infected and uninfected neurons were recorded either simultaneously, or sequentially with one recorded immediately after another with random order. Data was analyzed by Mini Analysis Program (Synaptosoft) with an amplitude threshold of 5pA for mEPSC analysis. To measure spontaneous spiking rate, neurons were patched in a cell-attached configuration in the presence of picrotoxin in ACSF. The pipette resistance ranged from 6 to 7 MΩ. The internal solution contained NaCl 118 mM, HEPES 10 mM. Each cell was recorded for 50 sweeps and each sweep lasted for 7 seconds. Data was analyzed by pClamp10 software.

Behavioral assays. All behavioral tests were conducted during the dark circadian period (18:00−23:00 for mice and 19:00-24:00 for rats).

The learned helplessness paradigm was conducted under dim light according to the previously optimized protocol (*15*). Experiments were performed on pair-housed cLH littermates or wild type SD rats. The paradigm contains two sessions. The "training session" consisted of 120 inescapable, uncontrollable electric foot shocks at 0.8mA over 40 min in the shocking chambers, with random shock durations and inter shock times ranging from 5 s to 15 s. Total shock duration was 20 min. The "testing session" was conducted 24hr after training, and learned helplessness phenotype was evaluated by a lever-pressing task, during which a cue-light-illuminated lever was added to the shocking chamber. This session consisted of 15 escapable shocks with 0.8 mA intensity and 24 s inter-trial intervals. Each shock lasted up to 60 s, but could be terminated by a lever pressing. Out of the 15 trials, more than 10 failures was defined as 'learned helplessness' (LH); less than 5 failures as 'non-learned helplessness' (NLH).

Forced swim test was conducted under normal light as previously described (*44*). Mice or rats were placed in a cylinder of water (temperature 23-25°C; 12 cm in diameter, 25 cm in height for mice; 20 cm in diameter, 40 cm in height for rats) for 6 min. The depth of water was set to prevent animals from touching the bottom with their hind limbs. For rats, there was an extra induction of 15-min swim in the previous day. Animal behavior was videotaped from the side. The immobility time of each animal spent during the last 4min of test was counted offline by an observer blind of the animal treatments. Immobility was defined as floating or remaining motionless, which means absence of all movement except motions required to maintain the head above the water.

For the sucrose preference test, mice were first single housed for 1 week, then habituated with two bottles of 1% sucrose for 3 days, followed by two bottles of water for 1 day (*45*). Then mice were water deprived for 24 h and then exposed to two bottles filled with either 1% sucrose or water for 2 h in the dark. The bottle position

was switched after 1 h. Total consumption of each fluid was measured and the sucrose preference was defined as the ratio of the consumption of sucrose solution versus the consumption of both water and sucrose solution during the 2 h test.

The elevated plus maze consisted of two open arms (30 × 6 cm), two closed arms (30 × 6 × 20 cm), and a central platform (6 × 6 cm). The maze was placed 50 cm above the floor in a room with normal lighting. Mice were individually placed in the central platform and allowed to explore the maze for 5 minutes. EthoVision video tracking system and software were used for recording and data analysis.

The open field test was conducted after all other behavioral tests. Mice were placed in the center of a plastic box (40 cm x 40 cm x 40.5 cm) in a room with dim light for 6 min. The testing arena was brightly lit. During session, animal behavior was videotaped and subsequently analyzed.

For chronic mild stress, group-housed male rats were exposed to a variable sequence of mild and unpredictable stressors (*46, 47*). A total of 13 different stressors were used over the course of three weeks. Stressors included isolation overnight, shaking 1 hour, light on overnight, white noise 2 hours, wet bedding overnight, titled cage overnight, restraint 2 hours, crowding overnight, food or water deprivation overnight, foot shock 40 min with random duration and interval, cold 1 hour, light off 3 hours, stroboscope overnight. Two stressors were used per day in a pseudo-random nature. Forced swimming test was used to measure depressive-like behaviors of animals.

Fig. S1

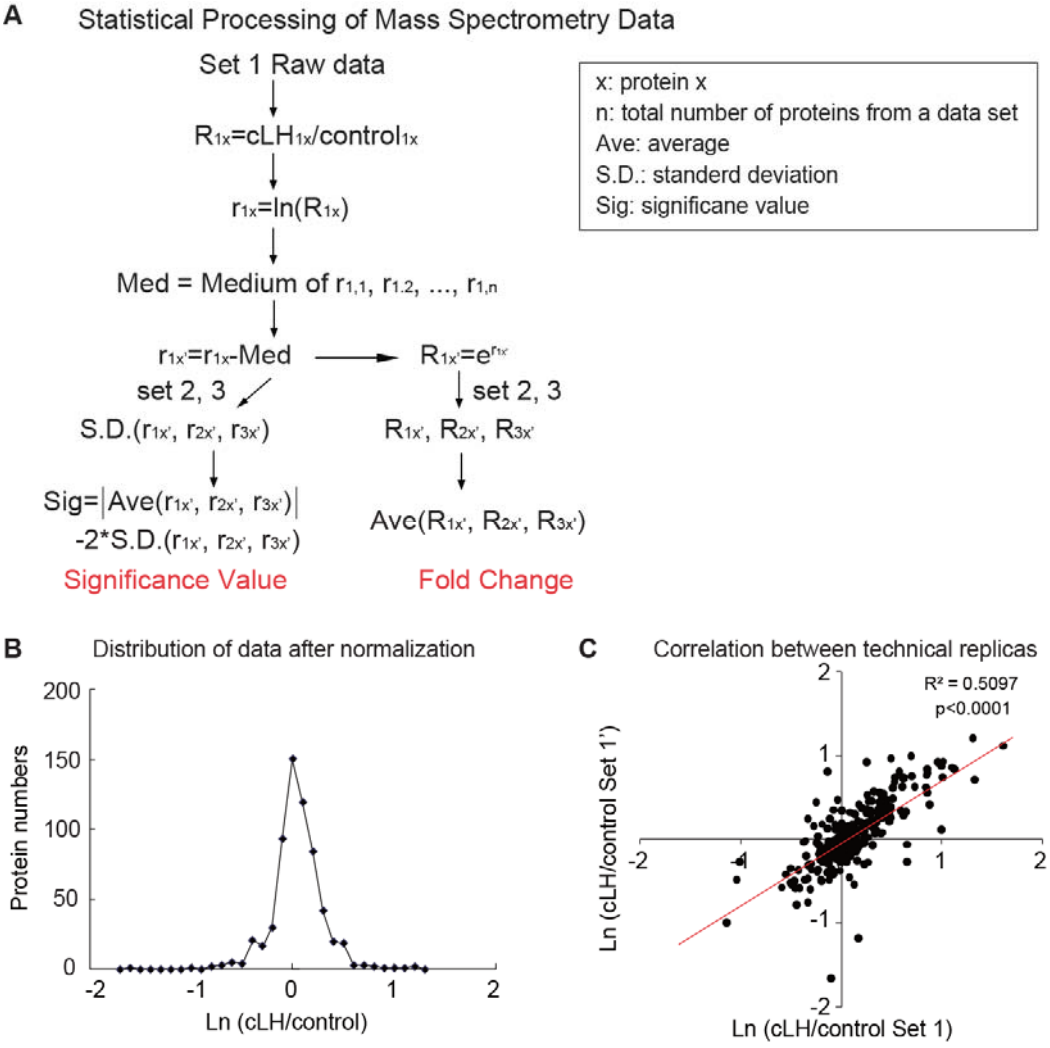

Fig. S1. Analysis of proteomic data sets. (**A**) Flow chart describing statistical data processing. Candidates with fold change > 50% and significance value > 0 were selected for further analysis. (**B**) Distribution of data after normalization. (**C**) To verify the technique, one set of samples was divided into two identical parts and ran twice on mass spec. Data from these two technical replicates were plotted against each other, and showed high correlation.

Fig. S2

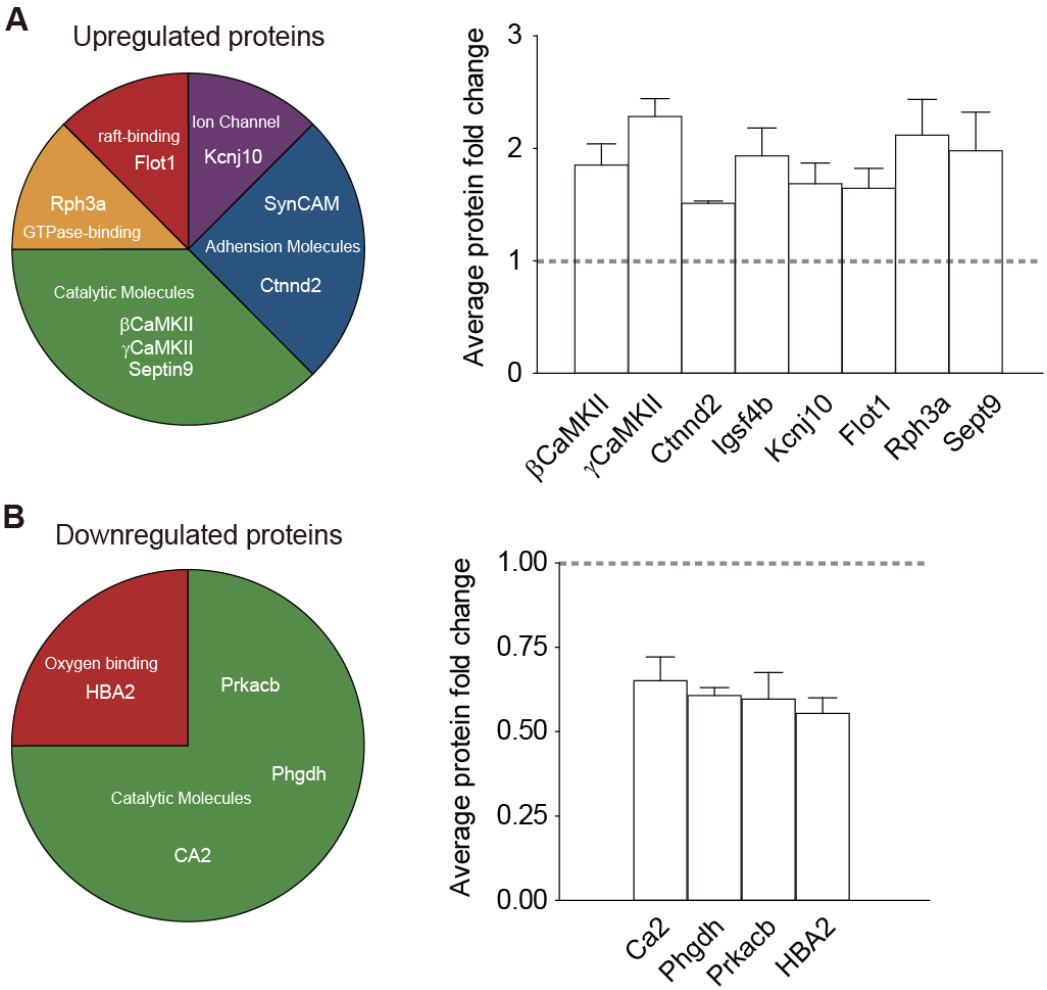

Fig. S2. Eight upregulated (**A**) and four downregulated (**B**) protein candidates identified by the proteomic screen. Note that most upregulated candidates are molecules enriched in the synapses, and most downregulated candidates are catalytic molecules involved in basic metabolic functions.

Fig. S3

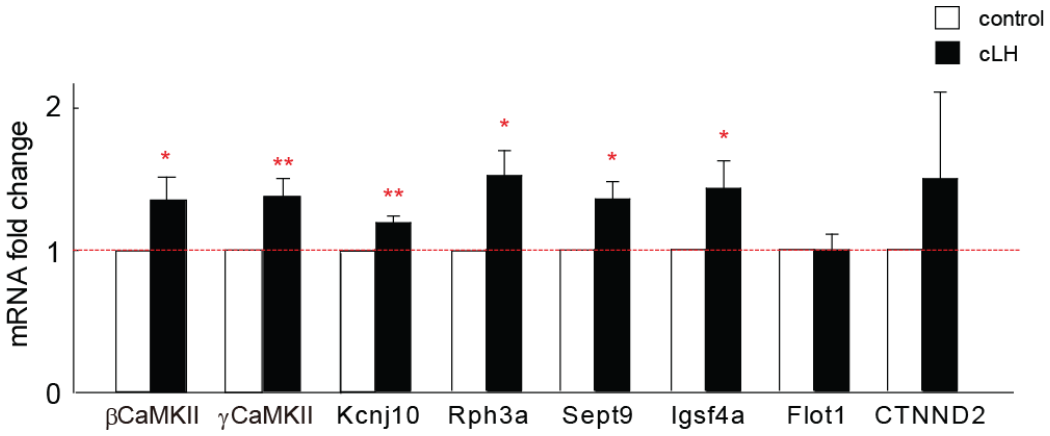

Fig. S3. QPCR verification of upregulated protein candidates. * $p < 0.05$， ** $p < 0.01$, two-tailed Students's *t* test.

Fig. S4

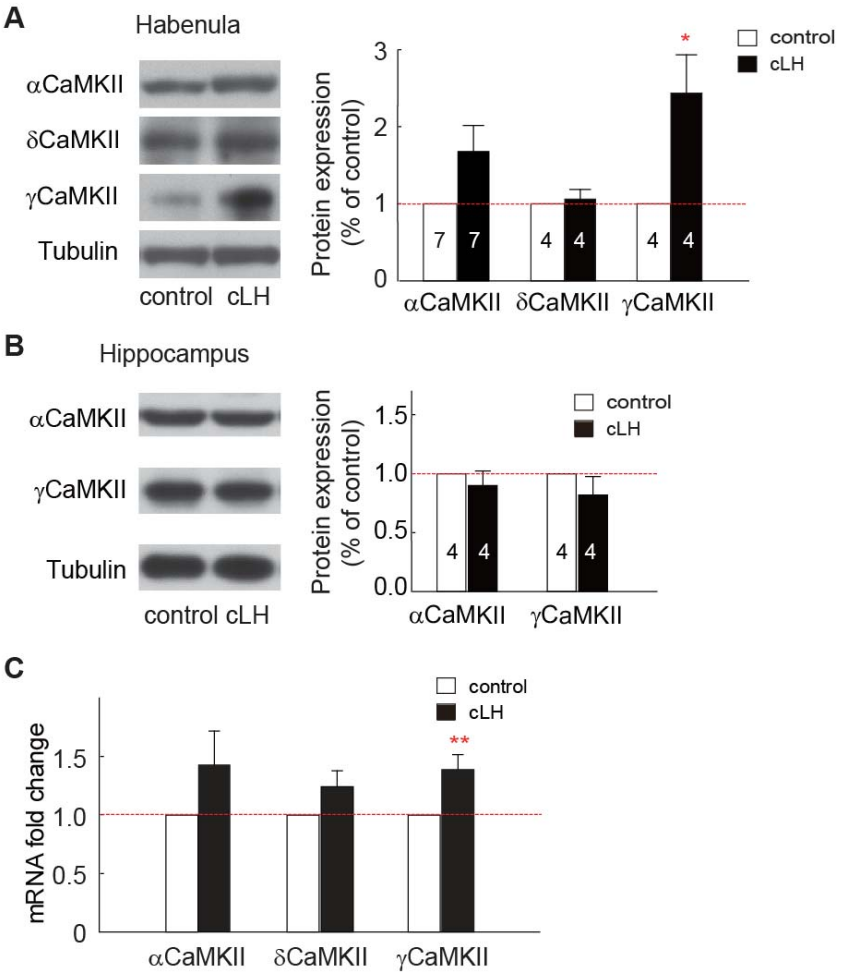

Fig. S4. Analysis of other three CaMKII family members. (**A**, **B**) Western blot analysis showing change of α-, δ- and γ-CaMKII in membrane fraction of habenula (**A**) or hippocampus (**B**) of cLH rats. (**C**) QPCR analysis of the habenular mRNA of the three CaMKII members. * $p < 0.05$， ** $p < 0.01$, two-tailed Students's *t* test.

Fig. S5

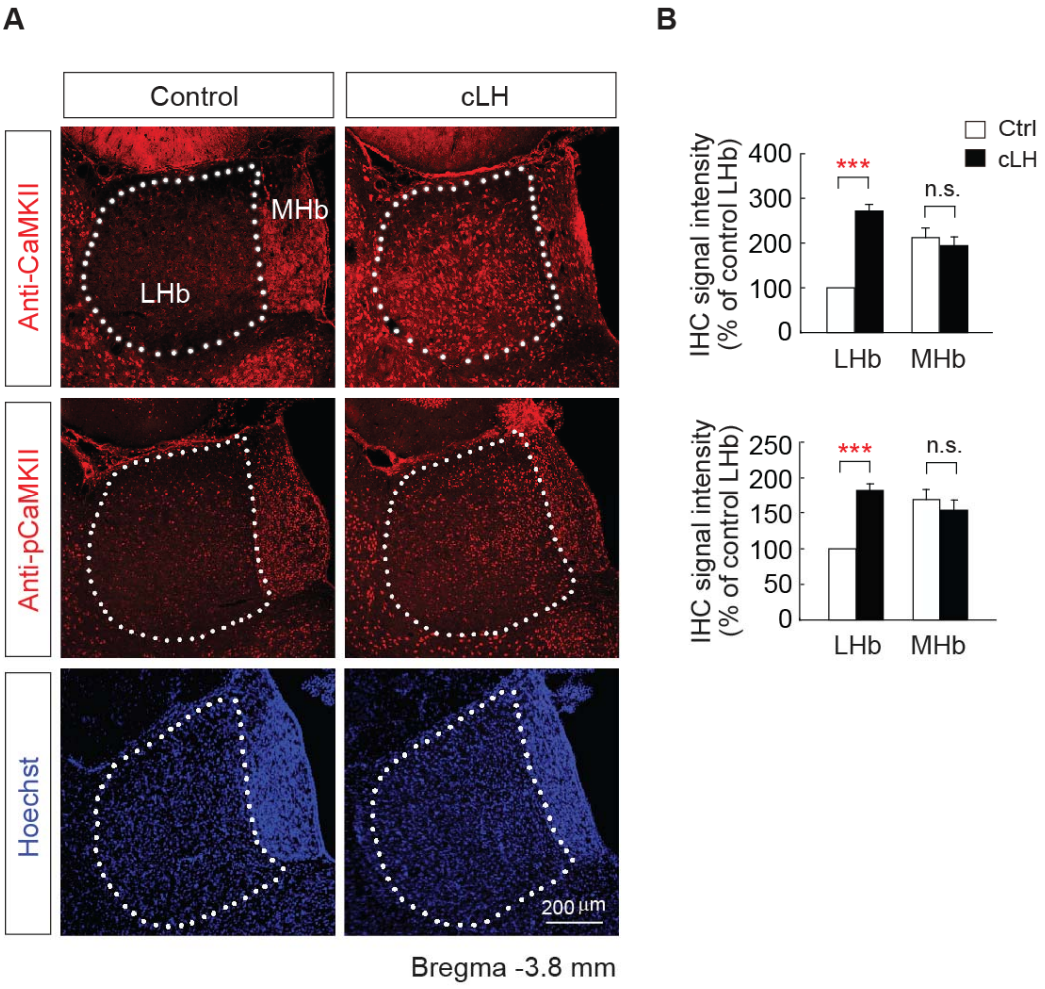

Fig. S5. Immunohistochemical analysis of CaMKII level in habenula. (A) Levels of both total CaMKII (top panel) and phospho-CaMKII (middle panel) were increased in the lateral part of habenula, LHb. A pan-CaMKII antibody was used here because we did not find a good βCaMKII-specific antibody for IHC. Note that the MHb in cLH is narrower than that in control rats. **(B)** Quantification of IHC signals in **(A)**. *** $p < 0.001$, two-tailed Students's *t* test.

Fig. S6

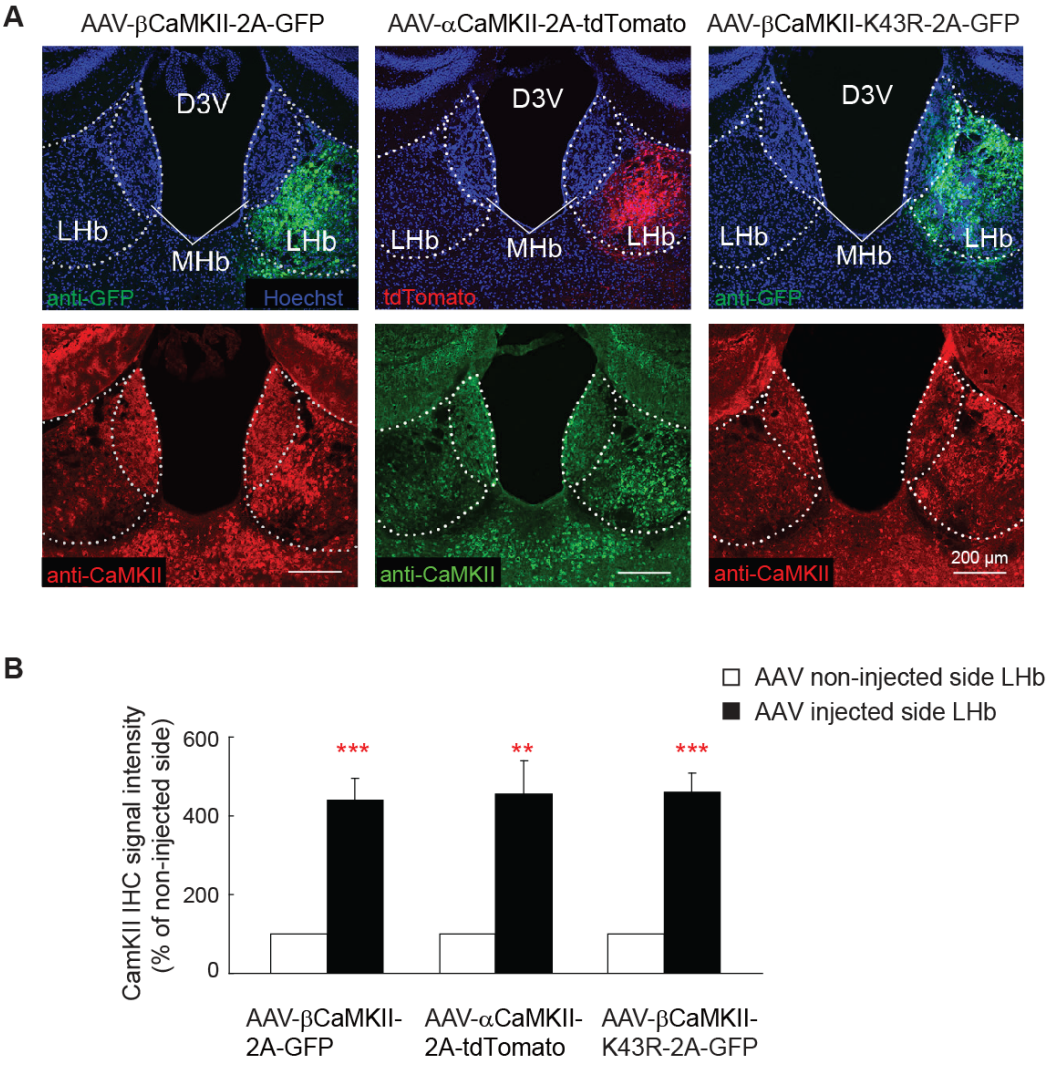

Fig. S6. Estimation of overexpression level of viral constructs through unilateral injection. (**A**) Pictures depicting coronal brain slices of mice that have received unilateral injection of three viruses. Top panels: Brain slices stained with anti-GFP (green) or directly visualized for tdTomato (red), counter-stained with Hoechst (blue). Left: non-injected side. Right: injected side. D3V: dorsal third ventricle. Bottom panels: Neighboring brain slices from same mice stained with anti-CaMKII antibody for quantification in (**B**). (**B**) Level of overexpression represented by ratio of CaMKII signal intensity of the injected and non-injected side. n=5 for AAV-βCaMKII-2A-GFP, n=4 for AAV-αCaMKII-2A-tdTomato and AAV-βCaMKII-K43R-2A-GFP. ** $p < 0.01$, *** $p < 0.001$, two-tailed Students's *t* test.

Fig. S7

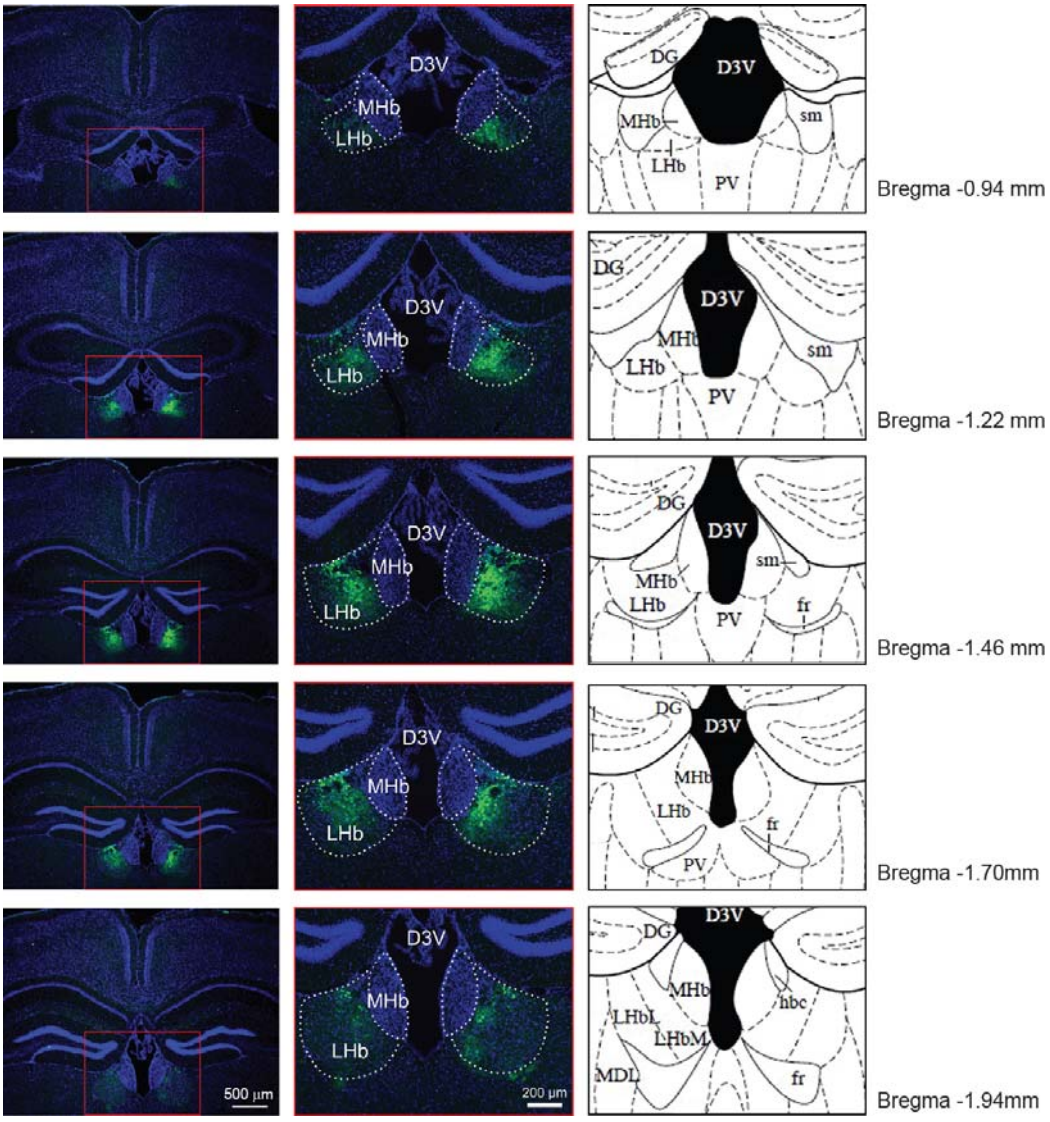

Fig. S7. Viral targeting in mouse LHb. Anterior-posterior positions where majority of the virus expression locates. Left are examples of brain slice taken from a mouse injected with AAV-βCaMKII virus. Middle are zoom-in images of the red square area in left. Right are corresponding schematics adapted from the atlas of Paxinos & Franklin 2004.

Fig. S8

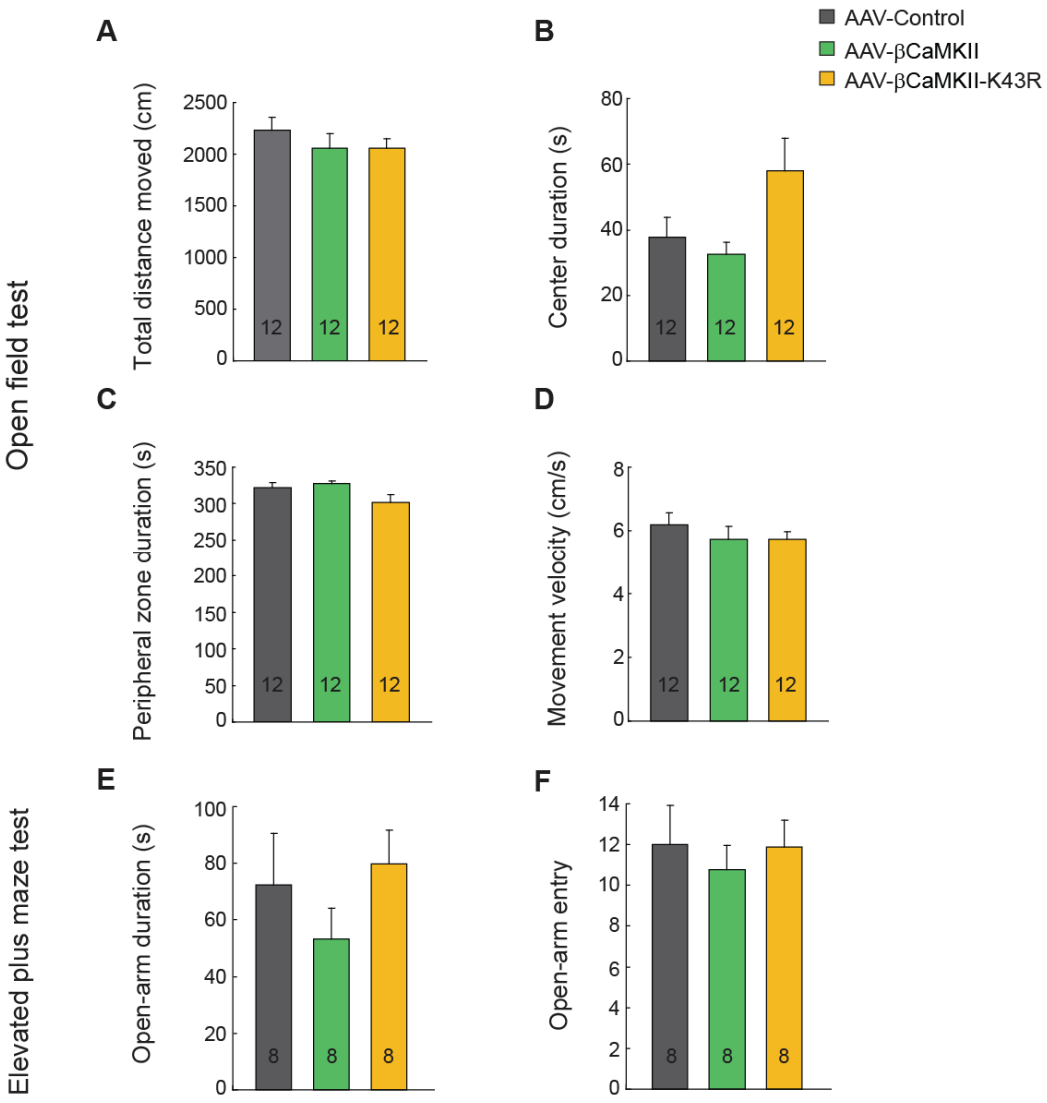

Fig. S8. Open field and elevated plus maze test of mice injected with different viruses. (**A-D**) Open field test. (**E, F**) Elevated plus maze test. No statistical difference was detected using one-way ANOVA with Bonferroni post hoc analysis.

Fig. S9

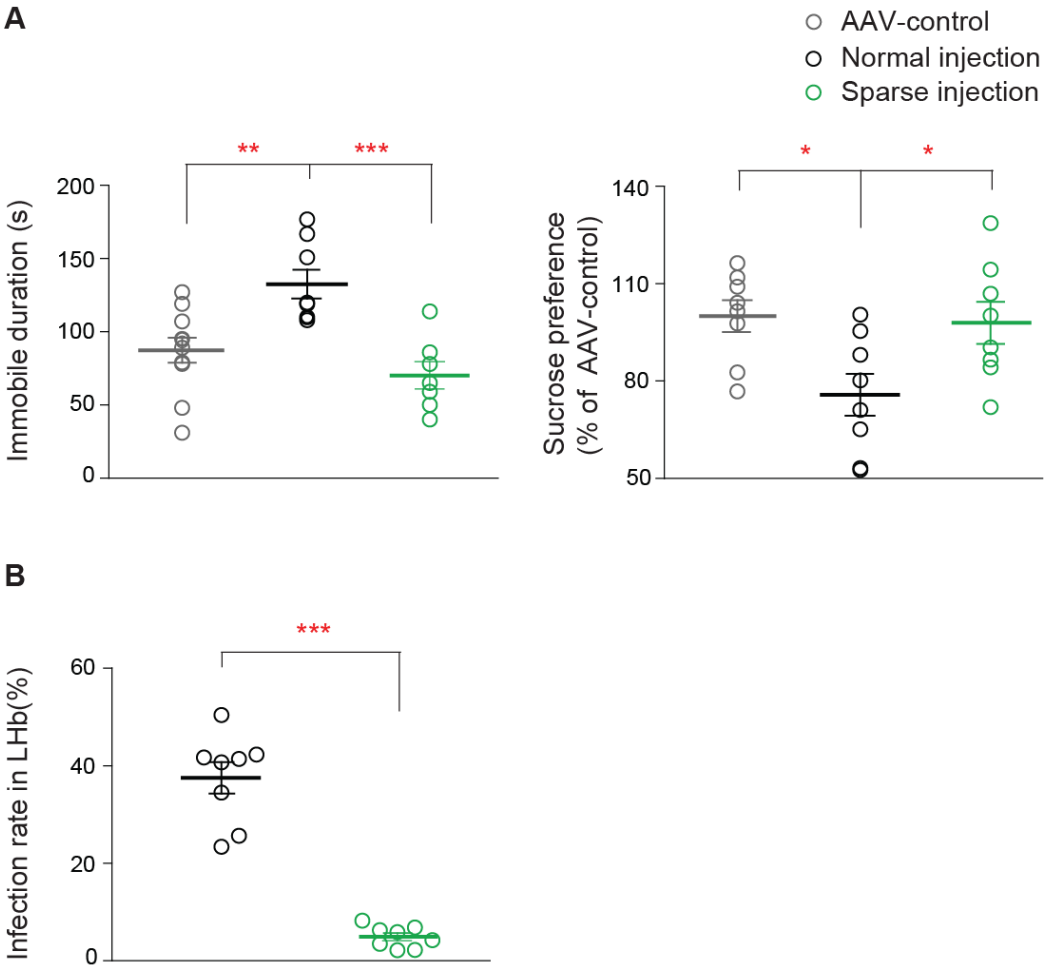

Fig. S9. Behavioral analysis of mice with normal or sparse injection of AAV-βCaMKII. (A) Immobility duration in the forced swim test (left) and sucrose preference (right). **(B)** Infection rate in LHb. *, $p<0.05$, ** $p < 0.01$， *** $p < 0.001$, one-way ANOVA with Bonferroni post hoc analysis.

Fig. S10

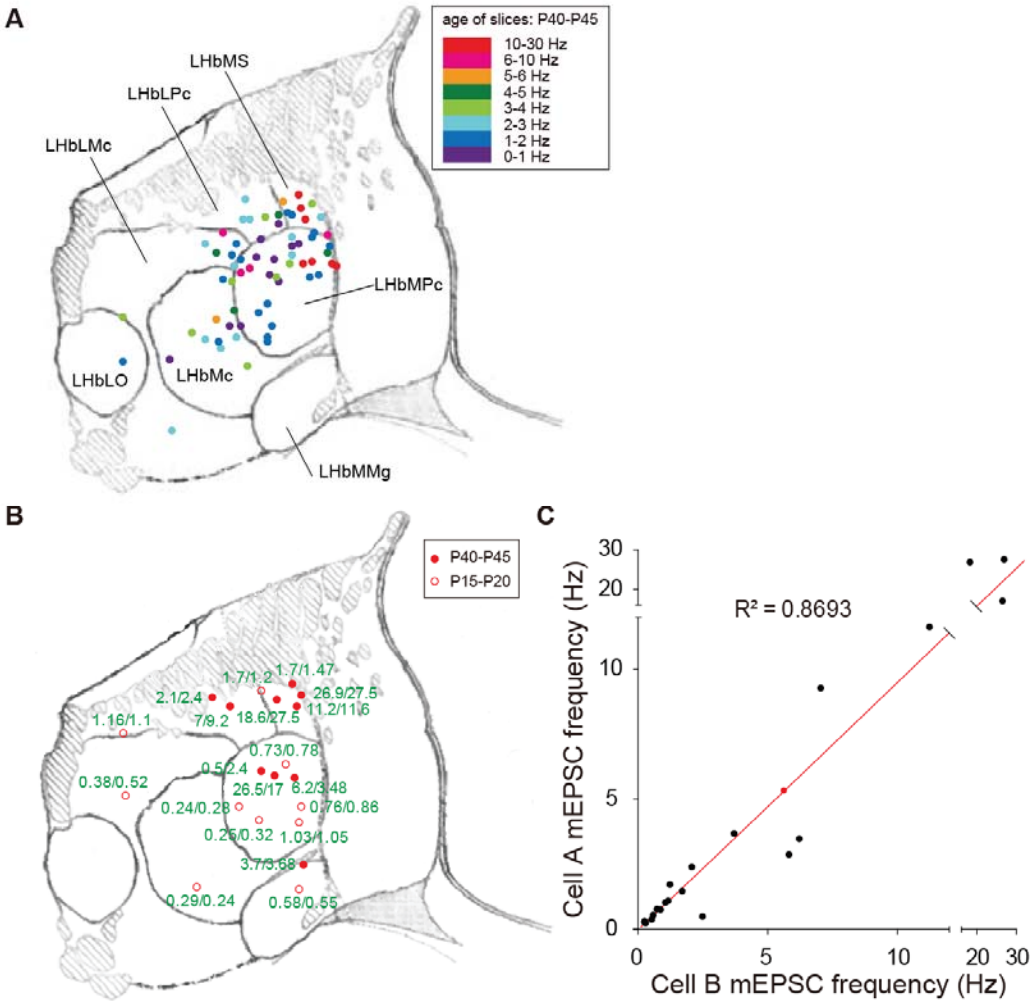

Fig. S10. Heterogeneous mEPSC response in LHb. (**A**) mEPSC recordings across different subregions of LHb. Each dot represents one neuron recorded. The frequencies of the mEPSC response are color-coded. (**B**) Each dot represents one pair of neurons recorded at that location. Values of the mEPSC frequency of each neuron pair are labeled. (**C**) mEPSC frequency of one neuron plotted against that of the other neuron from the same pair recorded in (**B**). Note that neurons from the same pair show highly similar mEPSC frequency despite variation from location to location.

Fig. S11

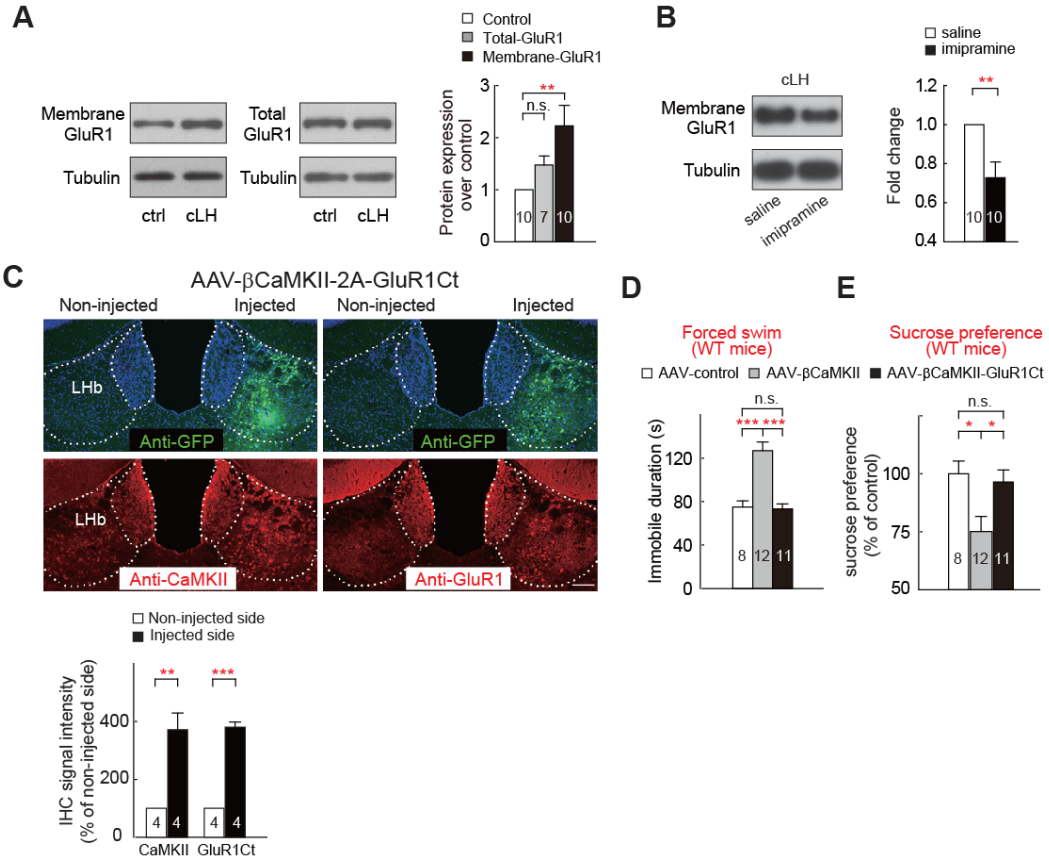

Fig. S11. Blocking synaptic incorporation of GluR1-type AMPA receptor, a molecule downstream of βCaMKII, alleviates depression. (**A**) Western blot analysis showing the level of GluR1 in the membrane fraction of habenular protein extract increased in cLH rats (**A**), and decreased after antidepressant imipramine treatment (**B**). (**C**) Co-expression of βCaMKII and GluR1Ct using an AAV-βCaMKII-2A-GluR1Ct virus increased immunohistochemistry signals of CaMKII and GluR1 in LHb. Bottom: quantification of IHC signal. Scale bars, 100 μm. (**D, E**) Co-expression of βCaMKII and GluR1Ct bilaterally in LHb blocked the forced swim (**D**) and anhedonia (**E**) phenotypes caused by βCaMKII over-expression. * $p < 0.05$, ** $p < 0.01$, *** $p < 0.001$, two-tailed Students's *t* test for (**B**) and (**C**), one-way ANOVA with Bonferroni post hoc analysis for (**A**) and (**D**).

Fig. S12

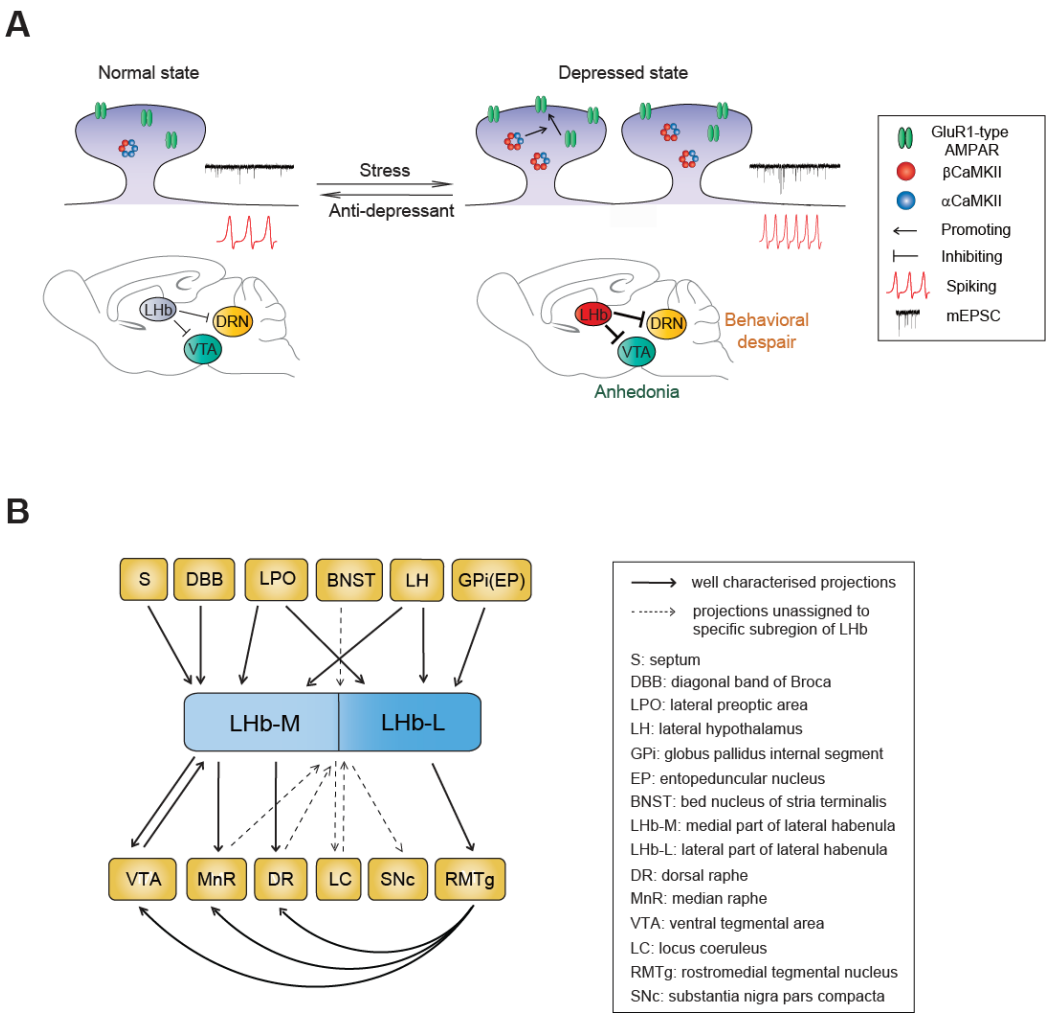

Fig. S12. (**A**) A model of depression based on LHb βCaMKII: In normal state, LHb has relative weak inhibition on VTA and DRN. In depressed state, stress causes upregulation of βCaMKII level, which leads to increased membrane trafficking of GluR1, increased synaptic efficacy and spike output of LHb neurons. As a result, the LHb inhibition onto VTA and DRN are enhanced, causing anhedonia and behavioral despair. (**B**) Afferent and efferent connections of LHb-M and LHb-L. LHb-M preferentially receives inputs from the septum (S), diagonal band of Broca (DBB) and dopamine neurons in the VTA (*48–51*). LHb-L preferentially receives inputs from the globus pallidus internus (GPi)/entopeduncular (EP) nucleus of the basal ganglia (*7*). The two subregions of LHb also receive selective inputs from different parts of lateral preoptic area (LPO) (*52*). In terms of downstream projections, LHb-M preferentially targets to VTA, median and dorsal Raphe, whereas LHb-L has more projections toward RMTg (*53*). However, such sub-divisional wiring analysis is not exclusive, and is sometimes incomplete.

Table. S1. Proteomic-derived expression level of 12 identified protein candidates. Student's *t*-test was performed on the log transformed fold change ratios.

Protein ID	Gene symbol	Fold-change cLH/ctrl	Set 1 ratio cLH/ctrl	Set 2 ratio cLH/ctrl	Set 3 ratio cLH/ctrl	p-value (Student's t-test)
Calcium/Calmodulin-Dependent Protein-Kinase II Beta	βCaMKII	1.85	2.21	1.78	1.57	0.002
Calcium/Calmodulin-Dependent Protein-Kinase II Gamma	γCaMKII	2.28	2.18	2.6	2.07	0.0001
Catenin (Cadherin-Associated Protein), Delta 2	Ctnnd2	1.51	1.54	1.53	1.47	0.00004
Synaptic Cell Adhesion Molecule 3	Igsf4b	1.93	NA	1.69	2.18	0.02
Potassium Inwardly-Rectifying Channel, Subfamily J, Member 10	Kcnj10	1.69	1.50	NA	1.87	0.02
Flotillin 1	Flot1	1.65	1.47	1.82	NA	0.02
Rabphilin-3A	Rph3a	2.12	NA	2.44	1.80	0.02
Septin-9	Sept9	1.98	1.64	2.32	NA	0.03
Carbonic Anhydrase II	Ca2	0.65	NA	0.65	0.72	0.03
Phosphoglycerate Dehydrogenase	Phgdh	0.61	0.58	NA	0.63	0.003
CAMP-Dependent Protein Kinase Catalytic Subunit Beta	Prkab	0.60	0.52	NA	0.68	0.03
Hemoglobin, Alpha 2	HBA2	0.55	0.51	0.60	NA	0.009

References and Notes

1. D. S. Charney, E. J. Nestler, *Neurobiology of Mental Illness* (Oxford Univ. Press, NewYork, 2005).

2. V. A. Vaidya, R. S. Duman, Depresssion—emerging insights from neurobiology. *Br. Med. Bull.* **57**, 61–79 (2001).

3. H. S. Mayberg, Modulating dysfunctional limbic-cortical circuits in depression: Towards development of brain-based algorithms for diagnosis and optimised treatment. *Br. Med. Bull.* **65**, 193–207 (2003).

4. D. Wirtshafter, K. E. Asin, M. R. Pitzer, Dopamine agonists and stress produce different patterns of Fos-like immunoreactivity in the lateral habenula. *Brain Res.* **633**, 21–26 (1994).

5. M. Matsumoto, O. Hikosaka, Lateral habenula as a source of negative reward signals in dopamine neurons. *Nature* **447**, 1111–1115 (2007).

6. O. Hikosaka, S. R. Sesack, L. Lecourtier, P. D. Shepard, Habenula: Crossroad between the basal ganglia and the limbic system. *J. Neurosci.* **28**, 11825–11829 (2008).

7. S. J. Shabel, C. D. Proulx, A. Trias, R. T. Murphy, R. Malinow, Input to the lateral habenula from the basal ganglia is excitatory, aversive, and suppressed by serotonin. *Neuron* **74**, 475–481 (2012).

8. A. M. Stamatakis, G. D. Stuber, Activation of lateral habenula inputs to the ventral midbrain promotes behavioral avoidance. *Nat. Neurosci.* **15**, 1105–1107 (2012).

9. S. Lammel, B. K. Lim, C. Ran, K. W. Huang, M. J. Betley, K. M. Tye, K. Deisseroth, R. C. Malenka, Input-specific control of reward and aversion in the ventral tegmental area. *Nature* **491**, 212–217 (2012).

10. A. Sartorius, K. L. Kiening, P. Kirsch, C. C. von Gall, U. Haberkorn, A. W. Unterberg, F. A. Henn, A. Meyer-Lindenberg, Remission of major depression under deep brain stimulation of the lateral habenula in a therapy-refractory patient. *Biol. Psychiatry* **67**, e9–e11 (2010).

11. S. Caldecott-Hazard, J. Mazziotta, M. Phelps, Cerebral correlates of depressed behavior in rats, visualized using 14C-2-deoxyglucose autoradiography. *J. Neurosci.* **8**, 1951–1961 (1988).

12. J. S. Morris, K. A. Smith, P. J. Cowen, K. J. Friston, R. J. Dolan, Covariation of activity in habenula and dorsal raphé nuclei following tryptophan depletion. *Neuroimage* **10**, 163–172 (1999).

13. J. Shumake, E. Edwards, F. Gonzalez-Lima, Opposite metabolic changes in the habenula and ventral tegmental area of a genetic model of helpless behavior. *Brain Res.* **963**, 274–281 (2003).

14. B. Li, J. Piriz, M. Mirrione, C. Chung, C. D. Proulx, D. Schulz, F. Henn, R. Malinow, Synaptic potentiation onto habenula neurons in the learned helplessness model of depression. *Nature* **470**, 535–539 (2011).

15. F. A. Henn, B. Vollmayr, Stress models of depression: Forming genetically vulnerable strains. *Neurosci. Biobehav. Rev.* **29**, 799–804 (2005).

16. S. F. Maier, Learned helplessness and animal models of depression. *Prog. Neuropsychopharmacol. Biol. Psychiatry* **8**, 435–446 (1984).

17. R. D. Porsolt, M. Le Pichon, M. Jalfre, Depression: A new animal model sensitive to antidepressant treatments. *Nature* **266**, 730–732 (1977).

18. L. Liao, S. K. Park, T. Xu, P. Vanderklish, J. R. Yates 3rd, Quantitative proteomic analysis of primary neurons reveals diverse changes in synaptic protein content in fmr1 knockout mice. *Proc. Natl. Acad. Sci. U.S.A.* **105**, 15281–15286 (2008).

19. N. E. Erondu, M. B. Kennedy, Regional distribution of type II Ca^{2+}/calmodulin-dependent protein kinase in rat brain. *J. Neurosci.* **5**, 3270–3277 (1985).

20. A. P. Braun, H. Schulman, The multifunctional calcium/calmodulin-dependent protein kinase: From form to function. *Annu. Rev. Physiol.* **57**, 417–445 (1995).

21. R. M. Sapolsky, The possibility of neurotoxicity in the hippocampus in major depression: A primer on neuron death. *Biol. Psychiatry* **48**, 755–765 (2000).

22. Y. I. Sheline, Hippocampal atrophy in major depression: A result of depression-induced neurotoxicity? *Mol. Psychiatry* **1**, 298–299 (1996).

23. P. Willner, Validity, reliability and utility of the chronic mild stress model of depression: A 10-year review and evaluation. *Psychopharmacology (Berlin)* **134**, 319–329 (1997).

24. H. Aizawa, M. Kobayashi, S. Tanaka, T. Fukai, H. Okamoto, Molecular characterization of the subnuclei in rat habenula. *J. Comp. Neurol.* **520**, 4051–4066 (2012).

25. K. Okamoto, R. Narayanan, S. H. Lee, K. Murata, Y. Hayashi, The role of CaMKII as an F-actin-bundling protein crucial for maintenance of dendritic spine structure. *Proc. Natl. Acad. Sci. U.S.A.* **104**, 6418–6423 (2007).

26. G. A. Wayman, H. Tokumitsu, M. A. Davare, T. R. Soderling, Analysis of CaM-kinase signaling in cells. *Cell Calcium* **50**, 1–8 (2011).

27. T. C. Thiagarajan, E. S. Piedras-Renteria, R. W. Tsien, α- and βCaMKII: Inverse regulation by neuronal activity and opposing effects on synaptic strength. *Neuron* **36**, 1103–1114 (2002).

28. D. G. Wheeler, C. F. Barrett, R. D. Groth, P. Safa, R. W. Tsien, CaMKII locally encodes L-type channel activity to signal to nuclear CREB in excitation-transcription coupling. *J. Cell Biol.* **183**, 849–863 (2008).

29. R. D. Groth, M. Lindskog, T. C. Thiagarajan, L. Li, R. W. Tsien, Beta Ca^{2+}/CaM-dependent kinase type II triggers upregulation of GluA1 to coordinate adaptation to synaptic inactivity in hippocampal neurons. *Proc. Natl. Acad. Sci. U.S.A.* **108**, 828–833 (2011).

30. S. H. Shi, Y. Hayashi, R. S. Petralia, S. H. Zaman, R. J. Wenthold, K. Svoboda, R. Malinow, Rapid spine delivery and redistribution of AMPA receptors after synaptic NMDA receptor activation. *Science* **284**, 1811–1816 (1999).

31. S. Rumpel, J. LeDoux, A. Zador, R. Malinow, Postsynaptic receptor trafficking underlying a form of associative learning. *Science* **308**, 83–88 (2005).

32. M. Popoli, M. Gennarelli, G. Racagni, Modulation of synaptic plasticity by stress and antidepressants. *Bipolar Disord.* **4**, 166–182 (2002).

33. G. Xing, S. Russell, C. Hough, J. O'Grady, L. Zhang, S. Yang, L.-X. Zhang, R. Post, Decreased prefrontal CaMKIIα mRNA in bipolar illness. *Neuroreport* **13**, 501–505 (2002).

34. T. Suenaga, S. Morinobu, K. Kawano, T. Sawada, S. Yamawaki, Influence of immobilization stress on the levels of CaMKII and phospho-CaMKII in the rat hippocampus. *Int. J. Neuropsychopharmacol.* **7**, 299–309 (2004).

35. G. Novak, P. Seeman, T. Tallerico, Increased expression of calcium/calmodulin-dependent protein kinase IIbeta in frontal cortex in schizophrenia and depression. *Synapse* **59**, 61–68 (2006).

36. J. Du, S. T. Szabo, N. A. Gray, H. K. Manji, Focus on CaMKII: A molecular switch in the pathophysiology and treatment of mood and anxiety disorders. *Int. J. Neuropsychopharmacol.* **7**, 243–248 (2004).

37. L. Brocke, L. W. Chiang, P. D. Wagner, H. Schulman, Functional implications of the subunit composition of neuronal CaM kinase II. *J. Biol. Chem.* **274**, 22713–22722 (1999).

38. K. Shen, M. N. Teruel, K. Subramanian, T. Meyer, CaMKIIbeta functions as an F-actin targeting module that localizes CaMKIIalpha/beta heterooligomers to dendritic spines. *Neuron* **21**, 593–606 (1998).

39. B. K. Lim, K. W. Huang, B. A. Grueter, P. E. Rothwell, R. C. Malenka, Anhedonia requires MC4R-mediated synaptic adaptations in nucleus accumbens. *Nature* **487**, 183–189 (2012).

40. D. Schulz, M. M. Mirrione, F. A. Henn, Cognitive aspects of congenital learned helplessness and its reversal by the monoamine oxidase (MAO)-B inhibitor deprenyl. *Neurobiol. Learn. Mem.* **93**, 291–301 (2010).

41. D. B. McClatchy, M. Q. Dong, C. C. Wu, J. D. Venable, J. R. Yates 3rd, 15N metabolic labeling of mammalian tissue with slow protein turnover. *J. Proteome Res.* **6**, 2005–2010 (2007).

42. M. P. Washburn, D. Wolters, J. R. Yates 3rd, Large-scale analysis of the yeast proteome by multidimensional protein identification technology. *Nat. Biotechnol.* **19**, 242–247 (2001).

43. A. Auricchio, M. Hildinger, E. O'Connor, G. P. Gao, J. M. Wilson, Isolation of highly infectious and pure adeno-associated virus type 2 vectors with a single-step gravity-flow column. *Hum. Gene Ther.* **12**, 71–76 (2001).

44. R. D. Porsolt, G. Brossard, C. Hautbois, S. Roux, Rodent models of depression: Forced swimming and tail suspension behavioral despair tests in rats and mice. *Curr. Protoc. Neurosci.* **Chapter 8**, Unit 8 10A (2001).

45. A. Towell, R. Muscat, P. Willner, Effects of pimozide on sucrose consumption and preference. *Psychopharmacology (Berlin)* **92**, 262–264 (1987).

46. R. D. Airan, L. A. Meltzer, M. Roy, Y. Gong, H. Chen, K. Deisseroth, High-speed imaging reveals neurophysiological links to behavior in an animal model of depression. *Science* **317**, 819–823 (2007).

47. M. Banasr, G. W. Valentine, X. Y. Li, S. L. Gourley, J. R. Taylor, R. S. Duman, Chronic unpredictable stress decreases cell proliferation in the cerebral cortex of the adult rat. *Biol. Psychiatry* **62**, 496–504 (2007).

48. M. Herkenham, W. J. Nauta, Afferent connections of the habenular nuclei in the rat. A horseradish peroxidase study, with a note on the fiber-of-passage problem. *J. Comp. Neurol.* **173**, 123–145 (1977).

49. L. Jennes, W. C. Beckman, W. E. Stumpf, R. Grzanna, Anatomical relationships of serotoninergic and noradrenalinergic projections with the GnRH system in septum and hypothalamus. *Exp. Brain Res.* **46**, 331–338 (1982).

50. O. T. Phillipson, C. J. Pycock, Dopamine neurones of the ventral tegmentum project to both medial and lateral habenula. Some implications for habenular function. *Exp. Brain Res.* **45**, 89–94 (1982).

51. O. Hikosaka, The habenula: From stress evasion to value-based decision-making. *Nat. Rev. Neurosci.* **11**, 503–513 (2010).

52. A. B. Kowski, S. Geisler, M. Krauss, R. W. Veh, Differential projections from subfields in the lateral preoptic area to the lateral habenular complex of the rat. *J. Comp. Neurol.* **507**, 1465–1478 (2008).

53. L. Gonçalves, C. Sego, M. Metzger, Differential projections from the lateral habenula to the rostromedial tegmental nucleus and ventral tegmental area in the rat. *J. Comp. Neurol.* **520**, 1278–1300 (2012).